Scientific Research Publishing

Open Journal of Polymer Chemistry, 2024, 14, 95-111
https://www.scirp.org/journal/ojpchem
ISSN Online: 2165-6711
ISSN Print: 2165-6681

Characterization and Performance of Magnesium Doped Bioactive Glass Nanoparticles

Anteneh Tilahun Awoke[1,2], Lingqi Zhu[1], Xinbo Ding[1*]

[1]College of Textile Science and Engineering, Zhejiang Sci-Tech University, Hangzhou, China
[2]Department of Textile Engineering, Ethiopian Institutes of Textile and Fashion Technology, Bahir Dar University, Bahir Dar, Ethiopia
Email: *dxblt@zstu.edu.cn

How to cite this paper: Awoke, A.T., Zhu, L.Q. and Ding, X.B. (2024) Characterization and Performance of Magnesium Doped Bioactive Glass Nanoparticles. *Open Journal of Polymer Chemistry*, **14**, 95-111.
https://doi.org/10.4236/ojpchem.2024.142005

Received: May 7, 2024
Accepted: May 28, 2024
Published: May 31, 2024

Abstract

The bioactive glass and related biomaterials have become increasingly popular, and have also attracted the research interest of many researchers in recent years due its special performance and tissue engineering application. In this study, to create a material with a variety of properties Mg doped hollow bioactive glass (Mg-HBG) of $80SiO_2$-$5P_2O_5$-10CaO-5MgO system had been produced by using a sol-gel method. The porous structure nanoparticles were specifically made by employing the cetyltrimethylammonium bromide (CTAB) as a surfactant. Magnesium was selected as a doped material with HBG, because it is the most existing cations in the human body which helps for bone metabolism as well as it has antibacterial property. Based on different investigations resulted nanoparticle with the inclusion of the lower molar fractions magnesium has good tested result. For a drug model vancomycin hydrochloride (VAN) was used in this study and it has also good antibacterial activity effect. These findings help the possibility of using Mg-HBG nanoparticles to treat infectious bone abnormalities by demonstrating their compatibility with antibiotics, drug loading and release behavior.

Keywords

Tissue Engineering, Bioactive Glass, Sol-Gel Process, Drug Loading and Release

1. Introduction

The bioactive glass materials are used in tissue engineering and regenerative medicine have been shown to have significant promise since the late 1990s [1].

During the development of the past 20 years would not have been feasible without the introduction of innovative designs and novel production methods. For a long time, Tissue Engineering (TE) research has focused on musculoskeletal tissues, including bone and cartilage, and every year, new clinical studies and experimental methods are proposed to evaluate new materials and scaffold designs [2]. Due to their behavior reaction with the physiological environment in an effective way by forming a strong bond interface of a bone-like hydroxyapatite, calcium phosphates, bioceramics, bioactive glasses, and other related materials which can be biodegradable material for bone regeneration of the scaffolds, to solve the constraints of traditional therapies biomaterial implantation for the tissue engineering [3]. A scaffold in general characterized as a 3-D structure that exhibits chemical, physical, and biological properties to promote cell adhesion, infiltration, and differentiation to the production of a mature and functional tissue.

Bioactive glass is now used as a reliable drug delivery system and a superior bone tissue regeneration material [4]. Hollow bioactive glass (HBG), with its exceptional *in vitro* bioactivity and well-ordered structure, has been a great contender for bone tissue regeneration. HBG with pore size distribution increase the surface area and large pore volume system of SiO_2-CaO-P_2O_5. When compared these glasses with non-hollow bioactive glasses, these characteristics show a greater bioactivity and degradability. The production of hollow bioactive glass that contain drug has allowed for the regulation of drug release kinetics and has the potential to remove negative effects associated with traditional medication delivery.

In this study, magnesium was doped with bioactive glass which helps for apatite formation and it leads to synthesis Mg-rich calcium phosphate layer [5] in the synthesis of SiO_2-CaO-P_2O_5-MgO system. Magnesium is an interesting element to use in bioactive glasses for medical applications because of its importance within the human body such as for stimulating the growth of new bone and is essential for bone metabolism, and its use to alter and improve the different properties (physical, thermal, mechanical) of the silicate bioactive glasses [6]. Magnesium It is hypothesized to interact with osteoblasts and oversee cell adhesion. Furthermore, it has been shown that a decrease in magnesium causes increased resorption, decreased growth, and bone loss, underscoring the mineral's function in bone metabolism [7].

For the treatment of the bone infections, medication molecules with strong antibacterial effectiveness and enhanced sterilizing effect are particularly important. The methicillin-resistant gram-positive bacteria, like Staphylococcus aureus which can be the cause of severe infections, and this can be treated with a tricyclic glycopeptide antibiotic of vancomycin hydrochloride (VAN) drug [8] [9]. This antibiotic also used for treatment of negative bacterial growth. Significantly, because of its hydrophilic nature of the VAN, the release behavior of carriers can be extended and maintained in the delivery systems [10].

This study used to synthesize and performance of magnesium doped bioactive glass scaffold for drug delivery of the bone repair application. Because of the porosity structure of the nanoparticle, the selected drug can pass along the channels even without requiring of the chemical bonding. Even though it should be ensured a local drug delivery system, this kind material should maintain a great capacity for loading drugs without experiencing the performance of degradation. The emphasis is on the creation of scaffolds with the necessary anatomical form and architecture using recently developed incorporated magnesium and hollow bioactive glasses. In these tissue engineering applications, the techniques for modifying the material's structure and the factors that have an impact on its performance were examined. The idea was to show that a cheap, easy technology could be used to create 3-D structures and different characterizations of the scaffold were studied

2. Materials and Methods

2.1. Materials

Deionized water (DI water), Cetyltrimethylammonium bromide (CTAB, Shanghai McLean Biochemical), Absolute ethanol (Hangzhou Shuanglin Chemical Reagent), Ammonia hydroxide ($NH_3 \cdot H_2O$, Shanghai McLean Biochemical Technology), Tetraethyl silicate (TEOS, Shanghai McLean Biochemical Technology.), Triethyl phosphate (TEP, Shanghai Aladdin Biochemical Technology), Calcium nitrate tetrahydrate (CaNT, Chengdu Kelong Chemical Reagent Factory), Vancomycin Hydrochloride (VAN, Shanghai Aladdin Biochemical Technology), Phosphate buffer solution (PBS, Homemade in the laboratory), Simulated body fluid (SBF, Homemade in the laboratory), magnesium chloride hexahydrate ($MgCl_2 \cdot 6H_2O$, Shanghai Mclean Biochemical Technology), Nutrient Agar (Hangzhou, China).

2.2. Preparation of Magnesium Doped Bioactive Glass (Mg-HBG)

First, 0.6 g CTAB was dissolved with a mixture of 165 mL deionized water and 78 mL ethanol at 37˚C and stir it. After stirring for two hours, 3 mL of ammonia was added. Next, 2.79 g TEOS, 0.30 g TEP, and 0.59 g CaNT were added at 2 hours intervals and stirred it until the solution to be cleared, followed by adding different amounts of magnesium chloride hexahydrate (Table S1) and stirred for 48 hours. Then white precipitates were centrifuged with rpm of 7000 for 7 minutes, washed with distilled water five times, and dried the sample at 60˚C. Finally, the dry white powder was calcined in electric box resistance furnace at 650˚C for 8 hours with a rate of 2˚C/min to completely remove the template agents in solution to obtain Mg doped HBG powder samples (donated as Mg-HBG nanoparticles) were collected. As indicated in Table S2, there are different mole compositions of bioactive glasses were made at room temperature for sol-gel preparation. Magnesium doped bioactive glass were fabricated by varying the amount of CaO and MgO, but other precursor reagents, the solvents

(ethanol, DI water, and ammonium hydroxide) and precursor reagents were maintained at constant values for comparison.

2.3. Physicochemical Characterization

The morphology and microstructure of HBG, Mg-HBG nanoparticles and SF/Mg-HBG electro spun scaffolds were analyzed by using Field emission scanning electron microscope (FESEM, Ultra-55, Carl Zeiss, German). The elemental distribution and chemical composition of the samples was tested by using electronic energy spectrometer (EDS, JSM-5610LV, Jeol, Japan), and the Fourier transform infrared spectroscopy (FTIR, Nicolet 5700, Thermo, USA) was used with the scanning range of 400 - 4000 cm^{-1}. The water contact angle (WCA) of the scaffold was measured by using contact angle meter (JCY series, Shanghai Fangrui, China), pH values was measured by pH meter (PHS-25, INESA, Shanghai, China). Mechanical properties of the electrospun composite scaffolds were tested by multifunctional mechanical testing machine (KES-G1, Shandong Xintiandi, China), absorbency of the solution was measured by UV spectrophotometer (UV-2600, Shanghai Jinghua, China).

2.4. Bioactivity Test in SBF

Bioactivity is a significant factor that can impact the performance of bone grafting materials. The study of the scaffold's bioactivity was carried out by immersing in SBF for 7 days with a pH value of 7.4 at 37˚C. The ability of the apatite formation on materials surface long SBF ion concentration in order to assess the materials' capacity attach to the bone. This shows the new bone formation on the scaffolds, *in vitro* apatite production is an essential a crucial step.

2.5. PH variation Measurements

During incubation process at different timepoints in SBF solution (1, 3, 5 and 7 days), pH variations were measured in order to examine the Mg-doped glasses' dissolving process. A pH meter that had been calibrated in accordance with internal standard operating procedures to monitor the pH values of the solution at the predetermined day.

2.6. Antibacterial Activity

S. aureus and *E. coli* bacteria types are used as a model for gram-positive and gram-negative bacteria respectively in order evaluating the antibacterial properties relating with different materials. Put the colony into a certain amount of nutrient broth and stir it several times to allow as many bacteria on the ring to enter the nutrient broth as possible. In a constant temperature shaker for 24 h. *S. aureus* and *E. coli* solution were used in saline solution. Dilute in proportion to the corresponding concentration range, and then take the diluted 1 mL S. aureus and *E. coli* bacteria respectively. Liquid, and 5 mg/mL of HBG, Mg-HBG nanoparticles were placed in a test tube of a constant temperature shaker for 24 h. Take out the test tube, use a pipette gun to put a certain number of bacteria into

the solid agar medium, and finally use the coating. The cloth rod spreads the bacterial liquid in the solid agar plate, and the bacterial liquid on the agar plate is no longer a stream. The liquid can be moved, and then the solid agar plate is placed in the constant temperature box of the bacteria for 24 hours. Last take the antimicrobial rate of the sample against the *S. aureus* and the *E. coli* was determined.

2.7. Drug Loading and Encapsulation Efficiency

The drug loading, and release characterizes of Mg-HBG nanoparticles was studied by using VAN as a model. The experimental procedures performed as; first 2 mg/mL solution was prepared (VAN mass/DI water). Next, 100 mg sample of Mg-HBG was mixed with 40 mL above VAN solution, and then stirred the solution for 24 h at 37˚C. Finally, the VAN loaded samples (denoted as VAN@Mg-HBG) were collected after centrifugation and dying. The solution absorbency was tested by UV-vis spectrophotometry at a wavelength of 280 nm and the concentration was calculated based on the standard curve of the drug. The sample's encapsulation efficiency and drug loading efficiency were calculated by using the following formula respectively.

$$\mathrm{EE}(\%) = \frac{\mathrm{Mb} - \mathrm{Ma}}{\mathrm{Mb}} \times 100$$

$$\mathrm{LE}(\%) = \frac{\mathrm{Mb} - \mathrm{Ma}}{\mathrm{Mc}} \times 100$$

where, Ma is the mass of drug in the superman (mg), Mb is the total mass of the drug added in to the system (mg), and Mc is the mass of the sample added into the carrier (mg).

2.8. Drug Release Kinetic Behavior

The drug release kinetic was investigated under two types of pH conditions by considering the wound's inflammatory stage. Briefly, 50 mg of VAN@HBG and VAN@Mg-HBG was added with 50 mL PBS solution with a pH of 1.2 and pH 7.4 levels at 100 rpm oribital shaking at 37˚C. 5 mL of the release PBS were taken out and 5 mL of fresh medium was replaced at prearranged intervals. The comulative release percentage of the drug from the samples was calculated by using the following equation [11].

$$\mathrm{Cmmulative\ percentage\ release}(\%) = \frac{\mathrm{volume\ of\ sample\ with\ drawal}(\mathrm{ml})}{\mathrm{Bath\ volume}(v)} xP(t-1) + Pt$$

where, Pt is the percentage release at time t, and $P(t-1)$ is the percentage release prior to time t.

3. Result and Discussion

3.1. Characterization of the Nanoparticles

Figure 1 shows the surface morphologies of Mg-HBG nanoparticles. It was

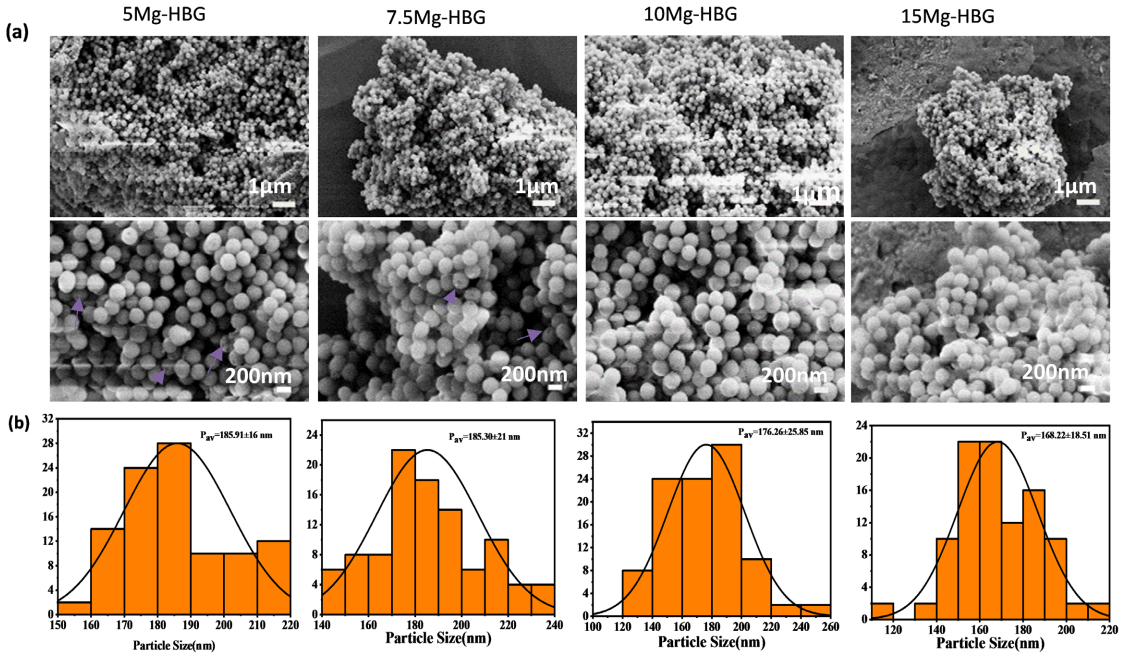

Figure 1. SEM micrographs (a) and corresponding particle size distribution (b) of Mg-HBG nanoparticles.

observed that on 5Mg-HBG, there was a uniformly distribution of the nanoparicle. This home homogeneous dispersion of Mg doped HBG increase the strength and enhance the pulling-out of the scaffold. When the amount of Mg was increased it was observed that the hollow structure was decreased and the agglemerated in the scaffold was observd (**Figure 1(a)**). Which means that the high surface unit volume of nanoparticls leads to strong attraction between particls to produce agglommeration.

The average particle size of nanoparrticles 5Mg-HBG, 7.5Mg-HBG, 10Mg-HBG and 15Mg-HBG are 185.91, 185.30, 176.25 and 168.22 nm respectively as shown in **Figure 1(b)**. When determining the particle size distribution with comparable solution concentrations and solvents, solution conductivity plays a valuable role. The average nanofibrous size increase with less concenration of Mg-HBG. This results in the scaffold not only reduces the potential increasemment of the mechanical properties in nanoparticles interconnection behavior, and also this is the cause of the deffect formation. As a result, the disperion properrties of Mg-HBG nanoparticles were an important for their reinforcing ability [12].

3.2. *In Vitro* Bioactivity

Figure 2 below shows the SEM pictures and EDS analysis of Mg-HBG nanoparticles after socking in SBF for 1 and 7 days. More cauliflower-like HA particles began to show up on 5Mg-HBG nanoparticle surface incubated in SBF for 1 day. During the experimental analyzed it was shown that many HA crystals structures then got denser on the surface particles. In this result, it was evident that with high amount of Ca and less amount of Mg particles used to improve the

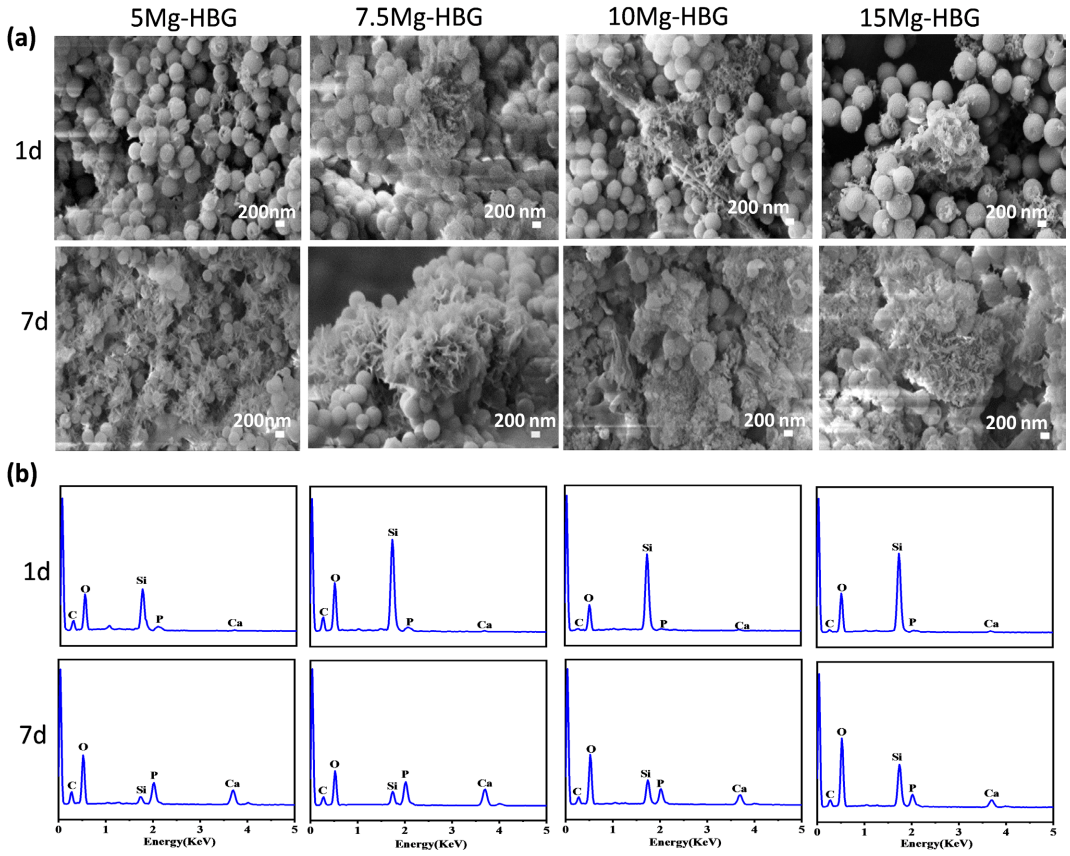

Figure 2. SEM micrographs (a) and EDS analysis (b) of Mg-HBG samples after soaking in SBF for 1 and 7 d.

bioactivity of the doped glass even further, but others growth rate of apatite was relatively slow. The increasement of HA formation on the surface of nanoparticles after soaked with SBF was corroborated by the increasing in calcium content, and phosphorous. While Mg-HBG with high Si content, it had evident that Mg-HBG nanoparticle released more Ca and Si to SBF medium, this is because of a high production of apatite on the bioactive glass surface.

3.3. FTIR Characterization

The samples' FTIR spectra following varying times of soaking in SBF are displayed in **Figure 3**. The peaks, which are related to the antisymmetric vibration of apatite in SBF. Furthermore, the spectra indicate the absorption at 560 and 600 cm^{-1}, which corresponds to the vibrational mode in a crystalline phosphate phase (P-O), following 1 and 7 days of soaking highly for 5Mg-HBG and suggesting a weakly crystallized hydroxyapatite phase [13]. However, after just 1 hours of immersion, the amorphous Ca-P that had already been deposited less shown crystallization in the 7.5Mg-HBG, 10Mg-HBG and 15Mg-HBG powders at 3200 - 3650 cm^{-1} (**Figure 3(a)**) but increase peak at 3450 cm^{-1} (**Figure 3(b)**) after 7 days of soaking. Based on these findings, we hypothesized that the inclusion of magnesium in the glass composition slows down the Ca-P layer that was developed during the initial phases of the bioactivity test.

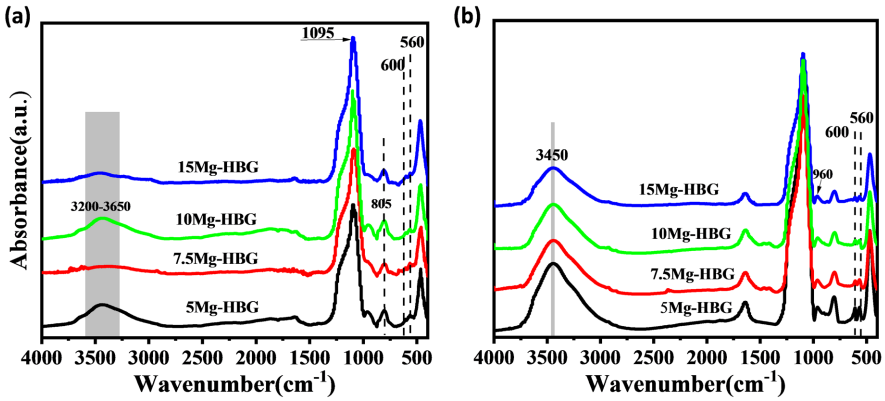

Figure 3. FTIR graph of Mg-HBG samples after soaking in SBF for 1 d (a) and 7 d (b).

3.4. pH Change Investigation

After the Mg-doped BGs were incubated for seven days, the pH variations in SBF were measured. The data presented in **Figure 4** indicates a notable increase specially at 5Mg-HBG (7.4 to 8.03) observed within the initial 24 hours of incubation. This rapid release of alkaline ions is consistent with the bioactivity mechanism proposed by Hench [14]. The HAp layer was gradually forming as the pH increased more gently until day 1, at which point it started to decline until day 3. After that, on days five through seven all the pH rises, but at early stage in the incubation period, there is a noticeable increase pH of the medium. This increasement is explained by the partial breakdown at the bioactive glass surfaces, since this type of biomaterial is very reactive [15]. In fact, there is an early-stage ion exchange between H_3O^+ from the SBF and Ca^{2+}/Mg^{2+} from the bioglass. By referring the previous research [16], it has been shown that Mg^{2+}might be deposited to the glass surface and alter the thermodynamic parameters, resulted in decreasing of the nucleation and crystal formation rates of hydroxy apatite from the amorphous calcium phosphate layer [17].

3.5. Antibacterial Activity Test

The gram-positive (*S. aureus*) and gram-negative (*E. coli*) bacterial were used in the matrix to evaluate the fabricated Mg-doped HBGs' antibacterial activity. MgO has antibacterial activity when bacterial cells interaction with nanoparticles, they leak their membranes, experience oxidative stress, and eventually lead to cell death [18]. **Figure 5(a)** shows the micrographs of blank *S. aureus* and *E. coli* bacterial culture and after they were revealed to the nanoparticles. It is evident that both bacterial colonies greatly decreased upon coming contact with HBG nanoparticles loaded with Mg, which is the quantity of Mg present was negatively correlated with the number of bacterial colonies [19]. Thus, it is possible to draw the conclusion that Mg loaded with HBGs can inhibit the development of bacteria than pure HBG. The inhibit percentage of *E. coli* and *S. aureus* following exposure to Mg-loaded nanoparticles is shown in **Figure 5(b)**. The inhibit percentage of both bacteria increased in all samples as the concentration

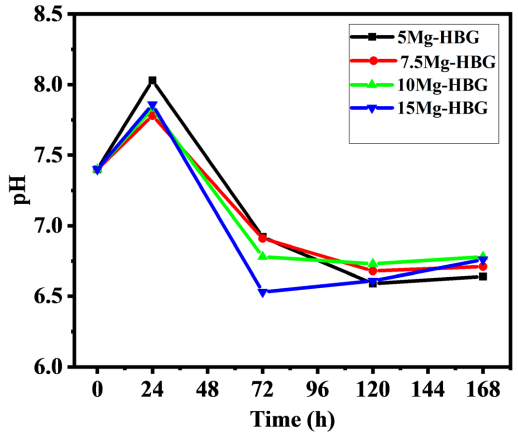

Figure 4. The graph of pH variations in SBF during 7 days soaking.

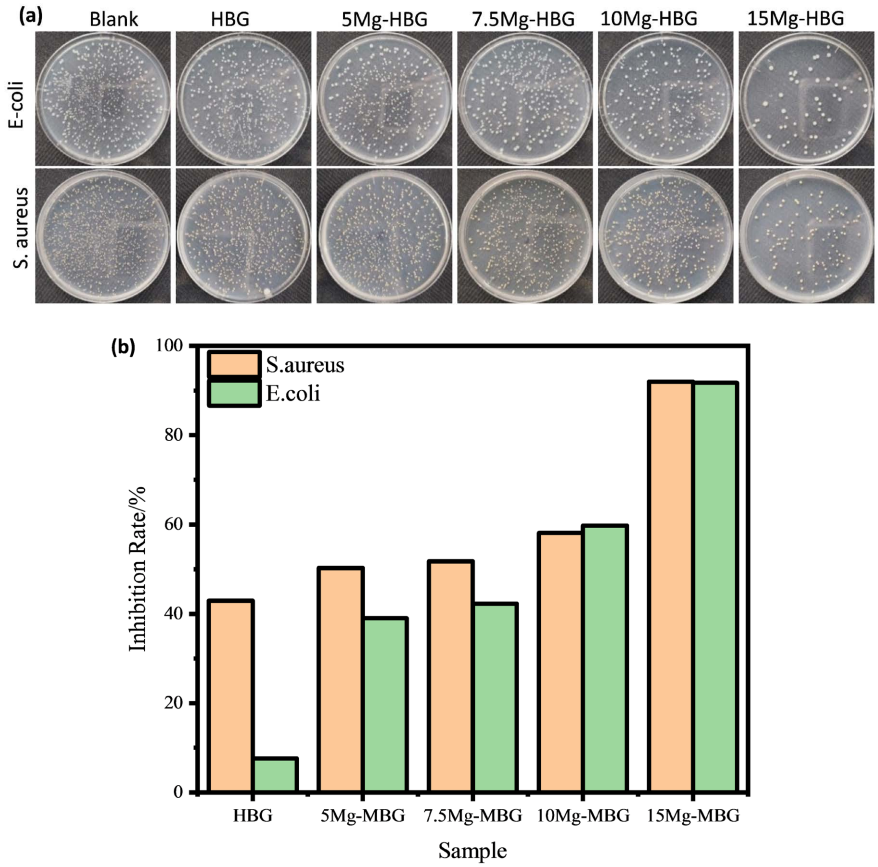

Figure 5. Photographs of antibacterial culture plates (a) and antibacterial inhibition rate (b) of *S. aureus* and *E. coli* on expose to Mg-HBG nanoparticles.

of Mg increased, suggesting that the antibacterial qualities of the samples loaded with Mg were progressively enhanced.

3.6. Drug Loading and Encapsulation Efficiency

In biological applications, the utilization of preparation nanoparticles for drug

delivery carrier is more significant. They make it possible to successfully encapsulate and distribute medications, such bone treatments, that have poor aqueous solubility profiles pH values. The drug of VAN was added to the Mg-HBG samples to get a high concentration in PBS solution. The encapsulation efficiency and the loading efficiency performance of the produced material is evaluated with regarding the applied drug during the experiment system in order to determine its effect on the applied part of the cell. As explained before, 5Mg-HBG had a significantly larger particle size than other Mg-HBGs, which may has helped explain why it had a greater drug loading efficiency and entrapment efficiency of up to 26.83% and 67.08% respectively. As shown in **Figure 6(a)**, the result of drug loading efficiencies and entrapment efficiency (**Figure 6(b)**) for 5Mg-HBGs, 7.5Mg-HBG, 10Mg-HBG and 15Mg-HBG slightly decreased with an increasement of magnesium. This is most probably for this reason is that due to decrees in particle size distribution on the nanoparticles.

3.7. VAN Release Kinetics Behavior

The release kinetics behaviors were studied according to the VAN@Mg-HBG was soaked in PBS at 37˚C for a week under the pH values of 1.2 and 7.4 (**Figure 7**) and monitored using UV-spectroscopy. It is shown that as time went on and VAN concentrations increased, less VAN was loaded into the Mg-HBGs, which in turn decreased the release rate. It was discovered that all release patterns were almost similar, including two phases: an initial rapid release phase and a subsequent constant release phase. In the initial phase, the VAN molecules that had some adhesion were released from the VAN@nMg-HBG nanoparticles' surface at pH 1.2, demonstrating the burst release within 12 h. After 12 h interaction with PBS solution, the release behavior of drug became slow and constant. Whereas, VAN@5Mg-HMBG continued to release VAN molecules to a considerable extent untill 24 h. On the other hand performing with pH 7.4 of SBF, the samples initially released highly increasing only within 4 h. After this, the release behavior of VAN-nMg-HBG nanoparticles slightly increased and then became slow and constant after 120 h. VAN@15Mg-HBG and 10Mg-HBG has low release rate compared with others respectively at both pH PBS solutions.

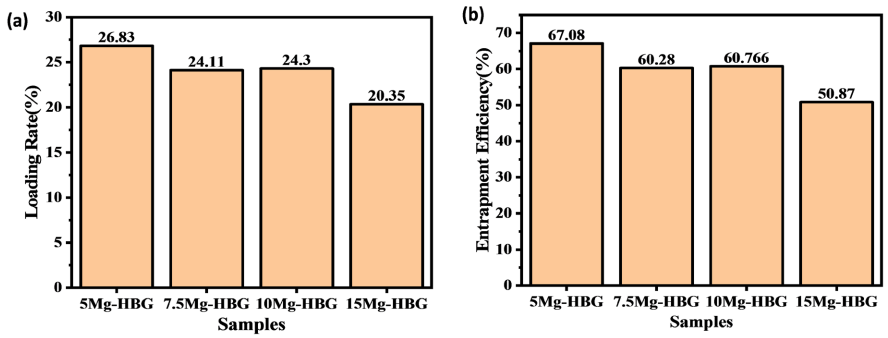

Figure 6. Drug loading efficiency (a) and (b) encapsulation efficiency (b) of Mg-HBG samples.

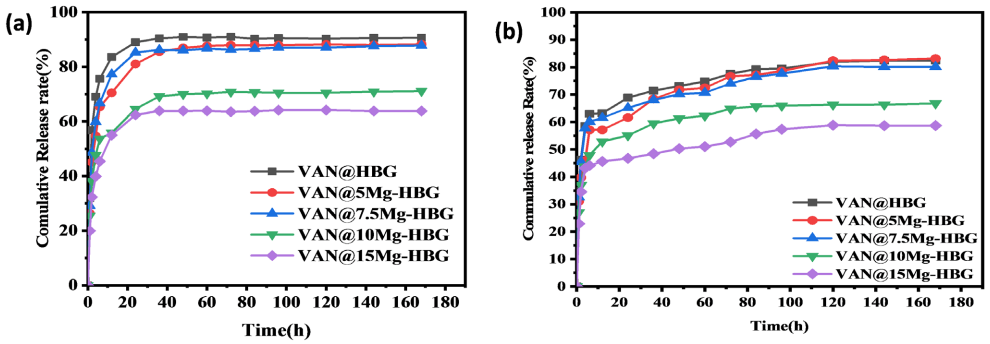

Figure 7. The cumulative VAN release percentage from VAN@Mg-HBG nanoparticles in two PBS solutions with pH values of 1.2(a) and 7.4(b).

The drug cumulative release rates at pH 1.2 (**Figure 7(a)**) of PBS were recorded as 89.61%, 83.39%, 82.31%, 67.36% and 60.62% for VAN@HBG, VAN@5Mg-HBG, 7.5Mg-HBG, 10Mg-HBG, and 15Mg-HBG, but for the pH of 7.4 (**Figure 7(b)**), it was 76.16%, 73.3%, 71.52%, 61.08%, 53.09% respectively. From these we understand that, the VAN commutative release quantity is higher at pH 1.2 PBS than pH 7.4. A rapid release rate can be caused by the release medium's acidity, which could help in the hydrophilic system of the VAN molecules' desorption from the Mg-HBG surface. The reason for the pH sensitivity of the VAN release rate could be the variation in hydrogen bond strengths between the silanol groups of HBGs and the hydroxyl groups and amino groups of VAN [20]. When compared to the other samples, it was evident that VAN@5Mg-HBG had a persistent and good drug-releasing behavior, which may have been caused by its unique hollow structure. This allowed the drug molecules to enter the hollow portion of the sample and ensured the drug release behavior of VAN@5Mg-HBG. The medication molecule could stick to the compacted Mg-HBG surfaces.

The release kinetics of VAN from the samples was investigated by using two varies pH solution. The first step data curves were fitted and analyzed by using Higuchi's square root model (**Figure 8(a)**, **Figure 8(b)**) [21], which is expressed as follows: $F_t = a_1 + k_1 t^{1/2}$, where t is the release time, k_1 is the release constant, and Ft is the fraction drug release at time t. Diffusion-controlled release was the mechanism used to release the hydrophilic VAN medicines encapsulated in the drug carriers. When VAN is exposed to PBS, it may physically be adsorbed on the Mg-HBGs' exterior surface and stay at the hollow window, which shows the VAN's first rapid release.

The first-order equation [22] that follows was used to analyze the data related to the second release level: Ln $(100 - F_t) = a_2 - k_2 t$ (**Figure 8(c)**, **Figure 8(d)**). Where Ft is the drug release at time t, $k_2$is release constant and t is the release time. Additionally, **Table S3** lists the fitted values of the correlation coefficient (R^2) and release constant (k) based on based on both equations at pH 1.2 and 7.4. During dissolution the Si-OH and P-OH groups on the surface HBG interact with the VAN molecules through hydrogen bonding as opposed to adsorption

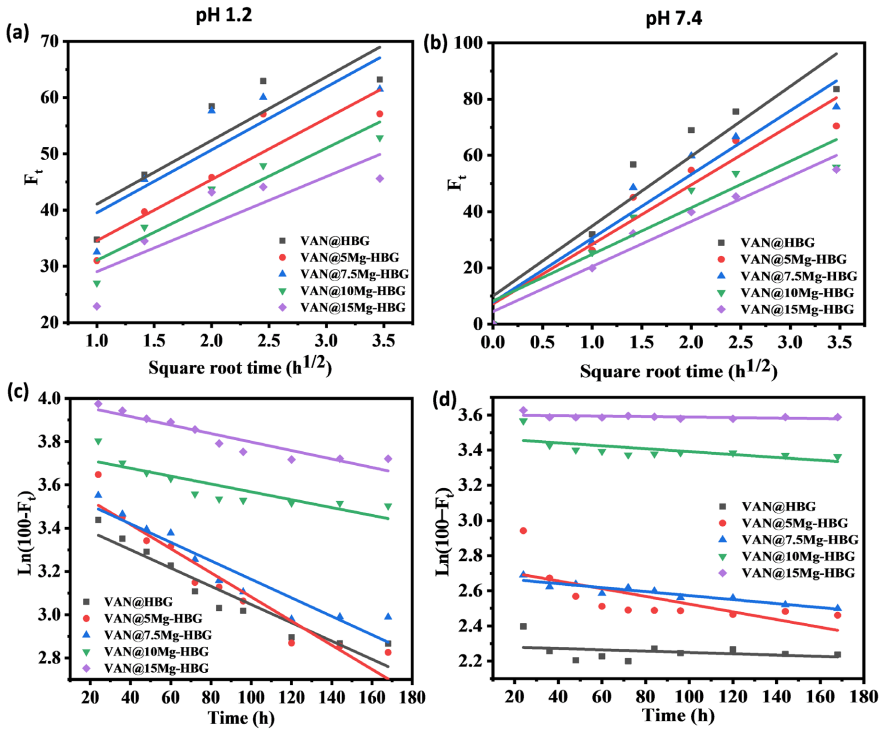

Figure 8. (a), (b) The first fast release stage of the linearized fitting profiles by using the Higuchi root model within 12 h in two PBS solutions with pH values of 1.2 and 7.4; (c), (d) the subsequent released stage of the linearized fitting profiles using first-order kinetic equations more than 12h in two PBS solutions with pH values of 1.2 and 7.4.

[23]. As a result, the strong contact brought by the adsorbed drug molecules may account for the slowing behavior in the release kinetics [24].

3.8. Antibacterial Activity of Drug to Nanoparticle

During this experiment *S. aureus* (gram positive) and *E. coli* (gram negative) bacteria in the matrix assessed the fabricated VAN-loaded samples' antibacterial activity. The micrographs of bacterial culture plates after they were exposed to the control (blank) and the drug-loaded of nanoparticles as shown in **Figure 9(a)**. Both bacteria were grown highly on the agar plate with control sample. But it is evident that the bacteria growth was decreased after the samples treated with VAN. Thus, it is possible to draw the conclusion that VAN could successfully inhibit the development of bacteria on samples. The inhibition rate of *E. coli* and *S. aureus* bacteria following exposure to VAN-loaded nanoparticles is shown in **Figure 9(b)**.

3.9. FTIR Study after VAN Loaded to the Nanoparticles

Figure 10 shows the FTIR spectrum of VAN with Mg-HBG samples in which the distinct peaks at 3415 cm^{-1} for the stretching of hydroxyl groups (O-H), 1658 cm^{-1} for the stretching of C=O and C, 1502 cm^{-1} for the C=C, and 1230 cm^{-1} for the hydroxyl groups of phenolics [25] (**Figure 10**), which overlap with the

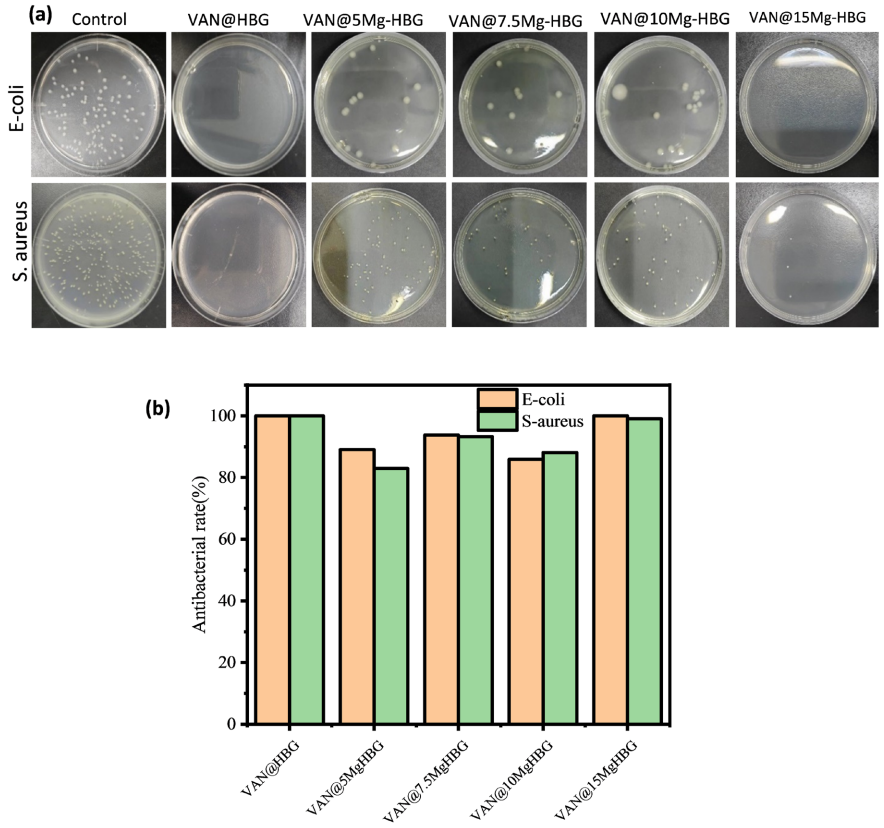

Figure 9. Antibacterial photograph of culture plates (a) and antibacterial inhibition rate (b) of *S. aureus* and *E. coli* exposed to VAN@Mg-HBG loaded samples.

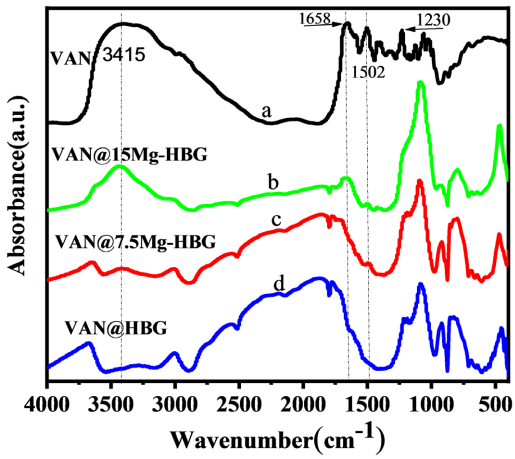

Figure 10. FTIR spectra of VAN and VAN@ Mg-HBG samples.

characteristic maxima of the HBG and Mg-HBG samples to a certain extent, which shows that VAN was successfully carried on the nanoparticles.

4. Conclusion

Bone damage is one of the most common medical conditions in the world today.

Bio glasses are one type of material that has been used for bone tissue engineering that exhibits excellent mechanical, cellular, and biocompatibility qualities. In this study, magnesium doped hollow bioactive glass nanoparticles were fabricated by using a sol-gel technique. The *in vitro* investigation of their bioactivity showed that the inclusion of magnesium at lower molar fractions into the glass network caused the glass to dissolve and become soluble quickly, as well as to have a delaying impact on the amorphous Ca-P layer's crystallization. Two more results from investigations into VAN loading and release were obtained. While the release kinetics increased according to a first order curve, the loading efficiency and entrapment efficiencies are also dropped as the magnesium level increased.

Acknowledgements

We acknowledge financial support from the Zhejiang Provincial Natural Science Foundation of China (Grant No.LQ23E030012); and the scientific Research Foundation of Zhejiang Sci-Tech University (Grant No.22202001-Y).

Conflicts of Interest

The authors declare no conflicts of interest regarding the publication of this paper.

References

[1] Muschler, G.F., Nakamoto, C. and Griffith, L.G. (2004) Engineering Principles of Clinical Cell-Based Tissue Engineering. *The Journal of Bone and Joint Surgery*, **86**, 1541-1558. https://doi.org/10.2106/00004623-200407000-00029

[2] Gerhardt, L. and Boccaccini, A.R. (2010) Bioactive Glass and Glass-Ceramic Scaffolds for Bone Tissue Engineering. *Materials*, **3**, 3867-3910. https://doi.org/10.3390/ma3073867

[3] Arepalli, S.K., Tripathi, H., Hira, S.K., Manna, P.P., Pyare, R. and Singh, S.P. (2016) Enhanced Bioactivity, Biocompatibility and Mechanical Behavior of Strontium Substituted Bioactive Glasses. *Materials Science and Engineering: C*, **69**, 108-116. https://doi.org/10.1016/j.msec.2016.06.070

[4] Bao, P., Kodra, A., Tomic-Canic, M., Golinko, M.S., Ehrlich, H.P. and Brem, H. (2009) The Role of Vascular Endothelial Growth Factor in Wound Healing. *Journal of Surgical Research*, **153**, 347-358. https://doi.org/10.1016/j.jss.2008.04.023

[5] Fernandes, H.R., Gaddam, A., Rebelo, A., Brazete, D., Stan, G.E. and Ferreira, J.M.F. (2018) Bioactive Glasses and Glass-Ceramics for Healthcare Applications in Bone Regeneration and Tissue Engineering. *Materials*, **11**, Article 2530. https://doi.org/10.3390/ma11122530

[6] Diba, M., Tapia, F., Boccaccini, A.R. and Strobel, L.A. (2012) Magnesium-Containing Bioactive Glasses for Biomedical Applications. *International Journal of Applied Glass Science*, **3**, 221-253. https://doi.org/10.1111/j.2041-1294.2012.00095.x

[7] Shoaib, M., Bahadur, A., Iqbal, S., AL-Anazy, M.M., Laref, A., Tahir, M.A., Channar, P.A., Noreen, S., Yasir, M., Iqbal, A. and Ali, K.W. (2021) Magnesium Doped Mesoporous Bioactive Glass Nanoparticles: A Promising Material for Apatite Formation and Mitomycin C Delivery to the MG-63 Cancer Cells. *Journal of Alloys and Compounds*, **866**, Article ID: 159013.

https://doi.org/10.1016/j.jallcom.2021.159013

[8] Hidayat, L.K., Hsu, D.I., Quist, R., Shriner, K.A. and Wong-Beringer, A. (2006) High-Dose Vancomycin Therapy for Methicillin-Resistant Staphylococcus Aureus Infections. *Archives of Internal Medicine*, **166**, 2138-2144. https://doi.org/10.1001/archinte.166.19.2138.

[9] Rai, A., Senapati, S., Saraf, S.K. and Maiti, P. (2016) Biodegradable Poly(ε-Caprolactone) as a Controlled Drug Delivery Vehicle of Vancomycin for the Treatment of MRSA Infection. *Journal of Materials Chemistry B*, **4**, 5151-5160. https://doi.org/10.1039/c6tb01623e

[10] Martínez-Vázquez, F.J., Cabañas, M.V., Paris, J.L., Lozano, D. and Vallet-Regí, M. (2015) Fabrication of Novel Si-Doped Hydroxyapatite/Gelatine Scaffolds by Rapid Prototyping for Drug Delivery and Bone Regeneration. *Acta Biomaterialia*, **15**, 200-209. https://doi.org/10.1016/j.actbio.2014.12.021

[11] Chandrasekaran, A.R., Jia, C.Y., *et al*. (2011) *In Vitro* Studies and Evaluation of Metformin Marketed Tablets-Malaysia. *Journal of Applied Pharmaceutical Science*, **1**, 214-217.

[12] Zhang, K., Wang, H., *et al*. (2010) Fabrication of Silk Fibroin Blended P (LLA-CL) Nanofibrous Scaffolds for Tissue Engineering. *Journal of Biomedical Materials Research Part A*, **93**, 984-993. https://doi.org/10.1002/jbm.a.32504

[13] Anna, L., Lao, J. and Josephine, L. (2013) Bioactive Glass Nanoparticles Obtained through Sol-Gel Chemistry. *Chemical Communications*, **49**, 6620-6622. https://doi.org/10.1039/c3cc00003f

[14] Hench, L.L. and Ethridge, E.C. (1982) Biomaterials: An Interfacial Approach. Academic Press, London.

[15] Mozafari, M., Banijamali, S., Baino, F., Kargozar, S. and Hill, R.G. (2019) Calcium Carbonate: Adored and Ignored in Bioactivity Assessment. *Acta Biomaterialia*, **91**, 35-47. https://doi.org/10.1016/j.actbio.2019.04.039

[16] Fiume, E., Migneco, C., Verné, E. and Baino, F. (2020) Comparison between Bioactive Sol-Gel and Melt-Derived Glasses/Glass-Ceramics Based on the Multicomponent SiO_2-P_2O_5-CaO-MgO-Na_2O-K_2O System. *Materials*, **13**, Article 540. https://doi.org/10.3390/ma13030540

[17] Souza, M., Crovace, M., *et al*. (2013) Effect of Magnesium Ion Incorporation on the Thermal Stability, Dissolution Behavior and Bioactivity in Bioglass-Derived Glasses. *Journal of Non-Crystalline Solids*, **382**, 57-65. https://doi.org/10.1016/j.jnoncrysol.2013.10.001

[18] He, Y., Ingudam, S., Reed, S., Gehring, A., Strobaugh, T.P. and Irwin, P. (2016) Study on the Mechanism of Antibacterial Action of Magnesium Oxide Nanoparticles against Foodborne Pathogens. *Journal of Nanobiotechnology*, **14**, Article No. 54. https://doi.org/10.1186/s12951-016-0202-0

[19] García-Alvarez, R., Izquierdo-Barba, I. and Vallet-Regí, M. (2017) 3D Scaffold with Effective Multidrug Sequential Release against Bacteria Biofilm. *Acta biomaterialia*, **49**, 113-126. https://doi.org/10.1016/j.actbio.2016.11.028

[20] Xia, W., Chang, J., Lin, J.P. and Zhu, J.Q. (2008) The pH-Controlled Dual-Drug Release from Mesoporous Bioactive Glass/Polypeptide Graft Copolymer Nanomicelle Composites. *European Journal of Pharmaceutics and Biopharmaceutics*, **69**, 546-552. https://doi.org/10.1016/j.ejpb.2007.11.018

[21] Higuchi, T. (1963) Mechanism of Sustained-Action Medication. Theoretical Analysis of Rate of Release of Solid Drugs Dispersed in Solid Matrices. *Journal of Pharmaceutical Sciences*, **52**, 1145-1149. https://doi.org/10.1002/jps.2600521210

[22] Anand, A., Das, P., Nandi, S.K. and Kundu, B. (2020) Development of Antibiotic Loaded Mesoporous Bioactive Glass and Its Drug Release Kinetics. *Ceramics International*, **46**, 5477-5483. https://doi.org/10.1016/j.ceramint.2019.10.264

[23] Kaur, G., Pandey, O.P., Singh, K., Chudasama, B. and Kumar, V. (2016) Combined and Individual Doxorubicin/Vancomycin Drug Loading, Release Kinetics and Apatite Formation for the $CaOCuO\text{-}P_2O_5SiO_2\text{-}B_2O_3$ Mesoporous Glasses. *RSC Advances*, **6**, 51046-51056. https://doi.org/10.1039/C6RA06829D

[24] Nawaz, Q., Fuentes-Chandia, M., Tharmalingam, V., Rehman, M.A., *et al.* (2020) Silibinin Releasing Mesoporous Bioactive Glass Nanoparticles with Potential for Breast Cancer Therapy. *Ceramics International*, **46**, 29111-29119. https://doi.org/10.1016/j.ceramint.2020.08.083

[25] Mohamed, H.B., El-Shanawany, S.M., Hamad, M.A. and Elsabahy, M. (2017) Niosomes: A Strategy toward Prevention of Clinically Significant Drug Incompatibilities. *Scientific Reports*, **7**, Article No. 6340. https://doi.org/10.1038/s41598-017-06955-w

Supplementary

Table S1. Amounts of Chemicals used for magnesium doped bioactive glass preparation.

Sample	TEOS (g)	TEP (g)	CaNT (g)	$MgCl_2 \cdot 6H_2O$ (g)
HBG	2.79	0.30	0.59	0
5Mg-HBG	2.79	0.30	0.39	0.17
7.5Mg-HBG	2.79	0.30	0.30	0.25
10Mg-HBG	2.79	0.30	0.20	0.34
15Mg-HBG	2.79	0.30	0	0.51

Table S2. Molar ratio of Magnesium doped bioactive glass.

Samples	SiO_2 (%mol)	P_2O_5 (%mole)	CaO (%mole)	MgO (%mole)	Molar composition
HBG	80	5	15	0	$80SiO_2$-$5P_2O_5$-15CaO
5Mg-HBG	80	5	10	5	$80SiO_2$-$5P_2O_5$-10CaO-5MgO
7.5Mg-HBG	80	5	7.5	7.5	$80SiO_2$-$5P_2O_5$-7.5CaO-7.5MgO
10Mg-HBG	80	5	5	10	$80SiO_2$-$5P_2O_5$-5CaO-10MgO
15Mg-HBG	80	5	0	15	$80SiO_2$-$5P_2O_5$-15MgO

Table S3. The values of K and R^2 for VAN@HBG and VAN@Mg-HBG.

			pH = 7.4		
Higuchi	VAN@HBG	VAN@5Mg-HBG	VAN@7.5Mg-HBG	VAN@10Mg-HBG	VAN@15Mg-HBG
K	24.85085	21.15365	22.7036	16.56719	16.0238
R^2	0.89741	0.91857	0.93048	0.88041	0.95572
			First order		
K	−0.00037556	−0.00219	−0.00113	−0.000829882	−0.000137107
R^2	0.10241	0.47871	0.88791	0.42735	0.21963
			pH = 1.2		
Higuchi	VAN@HBG	VAN@5Mg-HBG	VAN@7.5Mg-HBG	VAN@10Mg-HBG	VAN@15Mg-HBG
K	11.33105	10.87531	11.18698	9.98198	8.45964
R^2	0.77065	0.84933	0.75581	0.90155	0.72384
			First order		
K	−0.00422	−0.00558	−0.00428	−0.00182	−0.00196
R^2	0.91019	0.91397	0.89708	0.73153	0.87885